Austin Journal of Nanomedicine & Nanotechnology

Austin Publishing Group

Open Access Full Text Article

Research Article

Recent Development of Radiolabeled Nanoparticles for PET Imaging

Yan Xing[1,2], Jinhua Zhao [2]*, Xiangyang Shi[3], Peter S. Conti [1], Kai Chen [1]*

[1]Molecular Imaging Center, Department of Radiology, Keck School of Medicine, University of Southern California, USA
[2]Department of Nuclear Medicine, Shanghai First People's Hospital, Shanghai Jiao Tong University, China
[3]College of Chemistry, Chemical Engineering and Biotechnology, Donghua University, China

***Corresponding author:** Kai Chen, Molecular Imaging Center, Department of Radiology, Keck School of Medicine, University of Southern California, 2250 Alcazar Street, CSC103, Los Angeles, CA 90033, USA. Tel: 1 323-442-3858; Fax: 1- 323-442-3253; E-mail: chenkai@usc.edu. Jinhua Zhao, Department of Nuclear Medicine, Shanghai First People's Hospital, Shanghai Jiao Tong University, Shanghai 200080, China. E-mail: zjh1963@gmail.com

Received: January 06, 2014; Accepted: March 17, 2014; Published: March 24, 2014

Abstract

Nanoparticles bearing unique properties have gained great interest in biomedical applications. PET imaging can provide functional and molecular information on the biological events, offering the abilities to improve disease detection, therapeutic monitoring, and treatment efficacy. Nanoparticles labeled with a positron emitter can be used for PET imaging to noninvasively monitor their path and fate in living subjects. In the last few years, significant breakthrough has been made toward the application of various radiolabeled nanoparticles for PET imaging. This review briefly summarizes the recent development of radiolabeled nanoparticles, including organic and inorganic nanoparticles, for PET imaging in cancer and cardiovascular diseases. The major challenges involved in the translation of radiolabeled nanoparticles to the clinic PET are also discussed. It is expected that novel radiolabeled nanoparticles with PET along with other imaging modalities will afford accurate and precise assessment of biological signatures in a real-time manner and thus improve disease management.

Keywords: Radiolabeled nanoparticles; PET imaging; Cancer; Cardiovascular disease

Abbreviations

PET, Positron Emission Tomography; CT, Computed Tomography; MRI, Magnetic Resonance Imaging; NIRF, Near Infrared Fluorescence; NPs, Nanoparticles; EPR, Enhanced Permeability and Retention; CNTs, Carbon Nanotubes; SWCNTs, Single-Walled Carbon NanoTubes; MWCNTs, Multi-Walled Carbon Nanotubes; GO, Graphene Oxide; PEG, Polyethylene Glycol; GNPs, Gold Nanoparticles; QDs, Quantum Dots; IO, Iron Oxide; SPIO, SuperParamagnetic Iron Oxide; USPIO, Ultra-Small superParamagnetic Iron Oxide; RGD, Arg-Gly-Asp; pi, Postinjection; PBS, Phosphate Buffered Saline; PDGFR, Platelet-Derived Growth Factor Receptor; PDGFB, Platelet-Derived Growth factor B;GEMM, Genetically Engineered Mouse Model; PEO, Polyethylene Oxide; DOTA, 1, 4, 7, 10-tetraazacyclododecane-1, 4, 7, 10-tetraacetic acid; NOTA, 1,4,7-triazacyclononane-1,4,7-triacetic acid; DTPA, Dianhydridediethylenetriaminepentaacetic acid; CLIO, Cross-linked Iron Oxide; HSA, Human Serum Albumin; MPS, Mononuclear Phagocytic System

Introduction

Nanoparticles (NPs)usually refer to particles of sizes smaller than 100 nm [1]. A number of materials, including carbon, lipids, metals, metal oxides, polymers, silicates, and biomolecules can be prepared as nanoparticles with different shapes, such as spheres, cylinders, platelets, and tubes. Because of their unique physical properties, NPs demonstrate marvelous interactions with biomolecules. For instance, NPs with diameters ranging from 10 to 100 nm can extravasate through the endothelial cell layers and interact with the cell structures of various tissues due to the enhanced permeability and retention (EPR) effect. In addition, the large surface area to volume ratio renders NPs with the ability to be readily loaded with a variety of diagnostic and/or therapeutic agents as theranostics for disease detection and treatment.

Molecular imaging can be defined as *in vivo* visualization, characterization and measurement of biological processes at the molecular and cellular levels [2,3]. Up to date, various molecular imaging modalities have been exploited for disease diagnosis, stratification, and treatment assessment [4]. Molecular imaging involves administration of imaging probes and detection of signals produced from the probes [5]. Molecular imaging probes labeled with the prominent positron-emitter offer the opportunity to non-invasively monitor their path and fate in the living subject by the scintigraphic technique, positron emission tomography (PET). As an *in vivo* pharmacological imaging tool with the capability of providing highly sensitive and quantitative information, PET will play an increasingly important role in earlier disease detection and improved therapeutic decision making [6]. Due to their unique physical properties, NPs can be radiolabeled with positron emitting isotopes for noninvasively deciphering the biological events, such as tumor receptor levels and tumor enzyme activities [7]. Therefore, PET imaging using radiolabeled NPs has been attracting great interest in preclinical research and clinical setting [8,9]. However, the construction of radiolabeled nanoparticles is not trivial. Several key issues need to be taken into account, such as how to choose the appropriate isotopes and nanoparticles, what chemical reactions can be utilized to improve the labeling efficiency, and how to functionalize the nanoparticles to achieve the best contrast for PET imaging. Although several excellent reviews have been published

Citation: Xing Y, Zhao J, Shi X, Conti PS, Chen K. Recent Development of Radiolabeled Nanoparticles for PET Imaging. Austin J Nanomed Nanotechnol. 2014;2(2): 1016.

recently [9-11], very few of them focused on the construction method of radiolabeled nanoparticles and the key issues involved in the translation of radiolabeled nanoparticles to the clinic PET.

In this review, we address advantages and challenges in developing PET imaging probes by using different types of nanoparticles, and summarize the recent advances in the applications of radiolabeled nanoparticles for PET imaging of cancer and cardiovascular diseases.

Construction of PET radionuclide labeled nanoparticles

In order to obtain optimal imaging outcome, appropriate PET isotope and radiolabeling strategy must be carefully taken into consideration. The positron emitting isotopes can be generally classified into two classes according to their decay time. Short-lived positron emitters include ^{11}C ($t_{1/2}$ = 20 min), ^{15}O ($t_{1/2}$ = 2 min), ^{18}F ($t_{1/2}$ = 109.7min), ^{68}Ga ($t_{1/2}$ = 67.7 min), ^{64}Cu ($t_{1/2}$ = 12.7 hr), and ^{76}Br ($t_{1/2}$ = 16.2 hr) with half-lives from several minutes to hours. Typical long-lived positron emitters include ^{89}Zr and ^{124}I with half-lives of 3.2 days and 4.2 days, respectively [12]. Among these radionuclides, ^{64}Cu ($t_{1/2}$ = 12.7 h; β^+ 655 keV, 17.8%) has attracted considerable interest in the construction of radiolabeled NPs because of its favorable decay half-life, low β^+ energy, and commercial availability [13,14]. The PET radioisotope can be attached to the payload encapsulated inside the nanoparticle [15]. The radionuclide can also be conjugated directly on the surface of nanoparticle core through various labeling approaches, including direct labeling (nucleophilic or electrophilic reaction), indirect labeling (through prosthetic group), and coordination chemistry [7]. Among these approaches, complexation reactions of radiometal ions with chelates through coordination chemistry have been widely used. As compared to radio-halogenation, this approach has simpler chemistry and the production kits are usually commercially available. For example, 1, 4, 7, 10-tetraazacyclododecane-1, 4, 7, 10-tetraacetic acid (DOTA) is one of commonly used chelates for the construction of radiometal-labeled PET nanoparticles [16]. The typical radionuclides for PET imaging and the common radiolabeling methods [17-20] are summarized in Table 1.

PET radionuclide labeled nanoparticles

Carbon-based nanoparticles

The most popular carbon-based nanoparticles for biomedical applications include carbon nanotubes, graphene oxide nanoparticles, fullerenes and perfluorocarbon nanoemulsions. Carbon nanotubes (CNTs) are well-ordered hollow nanomaterials with lengths from several hundred nanometers to several micrometers. CNTs include single-walled carbon nanotubes (SWCNTs) with diameters of 0.4 to 2 nm and multi-walled carbon nanotubes (MWCNTs) with diameters of 2 to 100 nm. As one-dimensional nanomaterials, CNTs have attracted tremendous attentions in the field of biomedicine due to their unique physical and chemical properties. Positron emitting radionuclides can be conjugated or even inserted into CNTs for PET imaging. For example, McDevitt et al. synthesized ^{86}Y-CNTs from amine-functionalized and water-soluble CNTs by covalently attaching multiple copies of DOTA chelates and then radiolabeling with the positron-emitting metal-ion, yttrium-86 [21]. The whole-body PET images indicated that ^{86}Y-CNTs cleared from the blood within 3 h and predominantly distributed to the kidneys, liver, spleen, and bone in mice. Although CNTs are promising nanomaterials for diagnostic applications, CNTs are still considered with scepticism due to their perceived non-biodegradability. Different approaches have been thus developed to render this material biocompatible and to modulate any ensuing toxic effects [22].

Grapheneoxide (GO) is a class of two-dimensional sp^2-bonded carbon sheet which has attracted great attention in biomedicine because of its excellent electronic, thermal, mechanical, and optical properties. The functionalized GO nanoparticles with ultra-high surface area have been used as a nano-carrier for loading and delivery of various drugs and genes. The toxicity of GO is closely related to its surface chemistry. For example, PEG (polyethylene glycol) functionalized GO nanoparticles have shown minimal toxicity while administrated in mice [23]. Hong et al. developed ^{66}Ga-labeled nanographene for tumor vasculature imaging. GO nanoparticles with covalently linked, amino group-terminated six-arm branched PEG (10 kDa) chains were conjugated to NOTA (1,4,7-triazacyclononane-1,4,7-triacetic acid, for ^{66}Ga-labeling) and TRC105 (antibody binding to CD105, a biomarker for tumor angiogenesis) (Figure 1A). MicroPET imaging of 4T1 tumor-bearing mice showed that ^{66}Ga-NOTA-GO-TRC105 accumulated quickly in the 4T1 tumors and tumor uptake remained stable over time. Blocking studies with unconjugated TRC105 confirmed CD105 specificity of ^{66}Ga-NOTA-GO-TRC105, which was consistent with biodistribution and histology results (Figure 1B) [24]. Although the ^{66}Ga-labeled nanographene showed the tumor specificity, significant radioactivity was found in liver, which could be problematic for clinic translation.

Table 1: Representative radioisotopes and radiolabeling methods for the construction of radiolabeled nanoparticles for PET imaging.

PET Radioisotopes	Half life	Emission	Energy (KeV)	Radiolabeling Methods	Ref.
^{18}F	109.8 min	β^+	634	Direct (Nucleophilic or Electrophilic) or Indirect (Prosthetic) Labeling	[17]
^{64}Cu	12.7 h	β^-, β^+	579, 653	Coordination Chemistry	[18]
^{68}Ga	67.7 min	β^+	770, 1890	Coordination Cheemistry	[19]
^{124}I	4.18 days	β^+, γ	820, 1543, 2146	Nucleophilic Halogen Exchange Chemistry	[20]

Liposomes

Liposomes are spherical lipid bilayer nanoparticles enclosing an aqueous compartment that can accommodate lipophilic or hydrophilic drug molecules [25]. Due to the hydrophobic lipid bilayer surrounding aqueous core volume, liposomes are capable of encapsulating hydrophobic agents in the lipid shell, hydrophilic agents in the aqueous core, and amphiphilic agents distributed through the hydrophobic/hydrophilic domains. These unique properties make liposomes an excellent platform for the specific delivery of imaging moieties. Petersen et al. reported a rapid and feasible method to load radionuclide ^{64}Cu on PEGylated liposomes with high loading efficiency (95.5 ± 1.6%). A new ionophore, 2-hydroxyquinoline, was utilized to

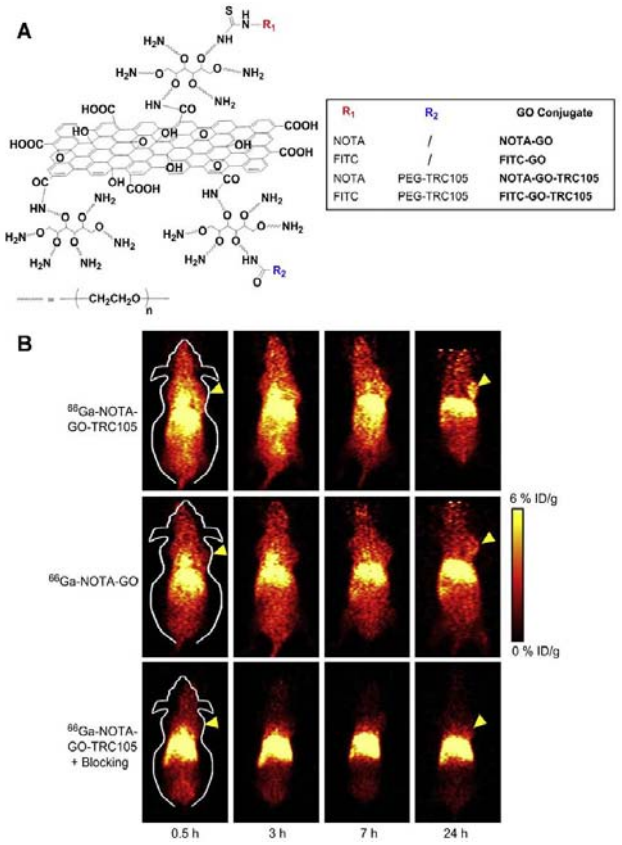

Figure 1: (A) Schematic representation of four nano-graphene conjugates. The NOTA chelator can be radiolabeled with ^{66}Ga. **(B)** Serial coronal PET images of 4T1 tumor-bearing mice at different time pointspostinjection of ^{66}Ga-NOTA-GO-TRC105, ^{66}Ga-NOTA-GO, or ^{66}Ga-NOTA-GO-TRC105 at 2 h after a blocking dose of TRC105. Tumors are indicated by arrows. Reprinted with the permission of the Biomaterials, Hong et al., 2012.

carry ^{64}Cu across the membrane of preformed liposomes and deliver it to an encapsulated copper-chelator [26,27]. MicroPET/CT images visualized an implanted colon adenocarcinoma in a mouse model at 24 h postinjection (pi). Biodistribution studies showed high tumor uptake (5.0%ID/g) at 24 h pi, which is consistent with the PET data. In another study, Emmetiere et al. reported a new approach by using bioorthogonal conjugation, the rapid reaction between tetrazines and trans-cyclooctenes. By coating ^{18}F radiolabeled liposomes with trans-cyclooctene and pretargeting with a tetrazine coupled to a targeted peptide, the retention of liposomes in tumor tissue was significantly enhanced. The reaction between tetrazines and trans-cyclooctenes was rapid. For *in vivo* PET imaging, ^{18}F radiolabeled liposomes exhibited fast clearance, low nonspecific binding, high signal-to-background activity ratios, and reduced toxicity to kidneys and bone marrow [27].

Gold nanoparticles

Gold nanoparticles (GNPs) are attractive for the construction of imaging agents due to their appealing properties, such as size controllability, good biocompatibility, and easy surface modification. Up to date, GNPs have shown great potential for application in PET, computed tomography (CT), Raman spectroscopy, and photoacoustic imaging. For example, Xie et al. reported a radiolabeled gold nanoshell for *in vivo* PET imaging in rats with tumor xenografts [28]. GNPs were coated with PEG2k-DOTA for ^{64}Cu chelation. The average radiolabeling efficiency was 81.3%, and ^{64}Cu-DOTA-GNPs were stable for 3 h in both phosphate buffered saline (PBS) and serum. PET scans at different times showed higher accumulation of ^{64}Cu-DOTA-GNPs in the tumor site, especially at 20 and 44 h pi as compared to ^{64}Cu-DOTA and ^{64}Cu-DOTA-PEG2k. In another study, ^{89}Zr-labeled antibody-targeted GNPs were proven a promising probe for cancer imaging and therapy [29]. Cetuximab, a chimeric human mouse anti-epidermal growth factor receptor monoclonal antibody, was functionalized with the desferal moiety and labeled with ^{89}Zr (^{89}Zr–Df–Bz–NCS–cetuximab) followed by a conjugation with GNPs using carbodiimide chemistry to afford AuNPs–PPAA–cetuximab–^{89}Zr. Radiolabeled cetuximab was conjugated to GNPs with a coupling reaction yield greater than 75%. *In vivo* PET imaging

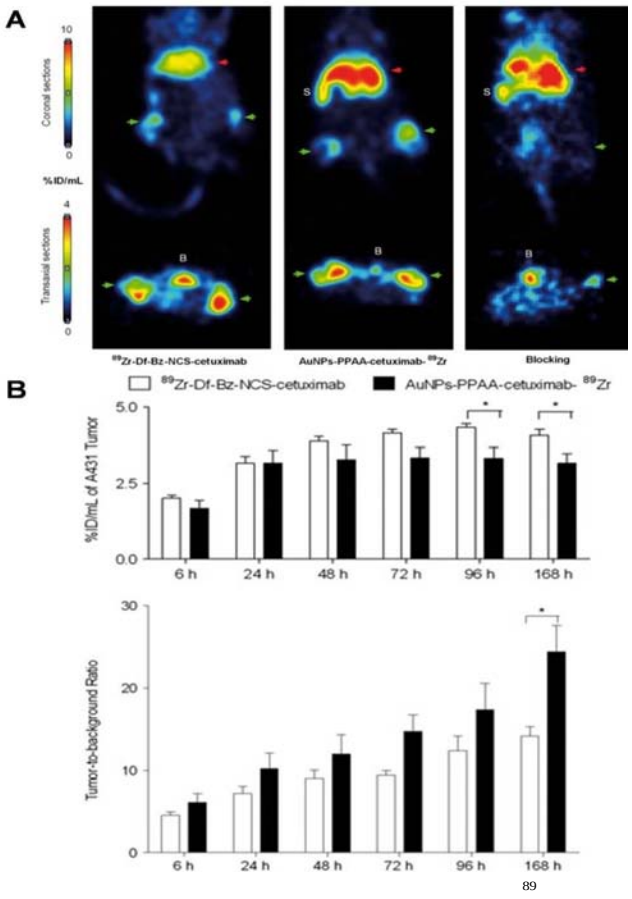

Figure 2: (A) A431-bearing nude mice, injected with ^{89}Zr–Df–Bz–NCS–cetuximab (**Left**), orAuNPs–PPAA–cetuximab–^{89}Zr (**Middle**) (two tumors per mouse), or AuNPs–PPAA–cetuximab–^{89}Zr 2 h after a blocking dose of unlabeled cetuximabouse (**Right**) (one tumor per mouse). Coronal (upper) and transaxial (lower) PET images were obtained 48 h after injection. Liver was shown as red arrows and tumors(bilateral) were indicated as green arrows. The bladder is indicated with 'B' and the spleen with 'S'. **(B)** Tumor uptake and tumor-to-background ratio of ^{89}Zr–Df–Bz–NCS–cetuximab or AuNPs–PPAA–cetuximab–^{89}Zr in A431-bearing nude mice at 6, 24, 48, 72, 96 and 168 h after injection. Reprinted with the permission of the Contrast Media &Molecular Imaging, Karmani et al., 2013.

was performed on A431 tumor-bearing mice at different time points to determine the probe uptake in tumor and liver. The results revealed no significant difference in tumor uptake for cetuximab conjugated to nanoparticles up to 72 h after injection as compared to unconjugated cetuximab. Immuno-PET studies showed that AuNPs–PPAA–cetuximab–^{89}Zr provided high tumor-to-background ratio (Figure 2). Although the liver uptake of AuNPs–PPAA–cetuximab–^{89}Zr was higher, compared with ^{89}Zr–Df–Bz–NCS–cetuximab, this study showed that the conjugation of GNPs to cetuximab did not affect its tumor accumulation. The ^{89}Zr-labeled cetuximab-targeted GNPs could be a valuable tool for theranostic purposes.

Metal oxide nanoparticles

Metal oxide nanoparticles have been widely applied in the construction of PET imaging probes. For instance, Perez-Campana and co-workers reported the activation of ^{18}O-enriched aluminum oxide (Al_2O_3) NPs by irradiation with protons to yield ^{18}F-labeled NPs via the ^{18}O(p,n)^{18}F nuclear reaction [30]. Biodistribution studies were performed in male rats using PET. The ^{18}F-labeled NPs allowed the determination of the biodistribution pattern in rodents up to 8 h after iv injection. A plateau was reached in the uptake of NPs in most of the organs within 1 h after administration. In addition, another strategy was recently presented from the same group to activate aluminum oxide (Al_2O_3) NPs by direct irradiation with protons via the ^{16}O(p,α)^{13}N nuclear reaction [31]. PET-CT imaging was utilized for biodistribution assay in male rats after iv administration of the probe. The accumulation of ^{13}N labeled NPs with different size in different organs was measured during the first 68 min after administration. The results showed that the uptake of NPs in the brain was very low irrespective of particle size. Relatively low accumulation of NPs (<2%) was observed in the lung for smaller NPs as compared to NPs with larger sizes. A high proportion of the NPs accumulated rapidly in the liver. More small NPs were trapped in the kidneys compared with larger NPs.

Radio labeled iron oxide is another major class of nanoparticle for PET imaging. The iron oxide NPs (IONPs) are typically classified by their sizes as standard superparamagnetic iron oxide (SSPIO) at 60–150 nm, ultra-small super paramagnetic iron oxide (USPIO) of approximately 5–40 nm, and mono crystalline iron oxide (MION) – a subset of USPIO ranging from 10 to 30 nm [7,32]. Among these IONPs, the SPIONPs have unique properties such as biocompatibility and intrinsic ability to facilitate surface modification, making them attractive as multifunctional imaging agents. Recent applications of radiolabeled iron oxide nanoparticles for PET imaging and multimodality imaging have been previously summarized in comprehensive reviews [33,34].

Micelles

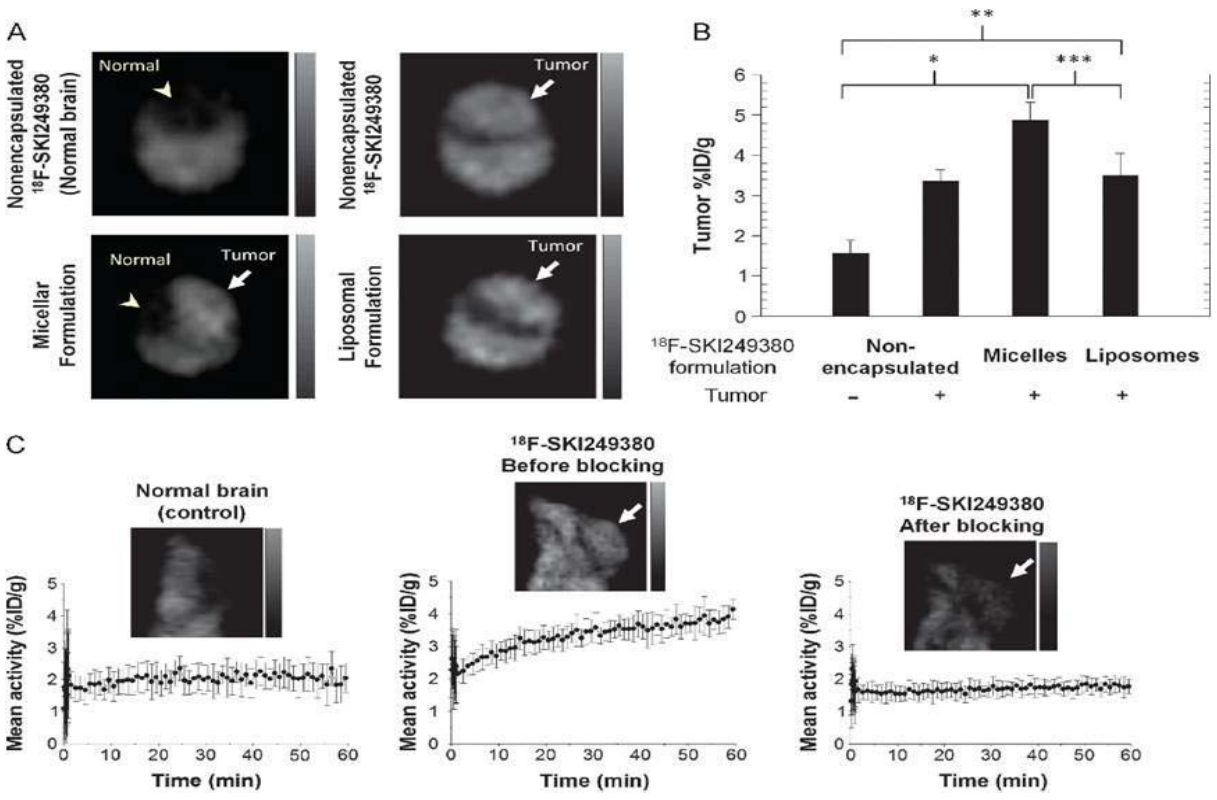

Figure 3: (A) Representative axial microPET images at 1 h pi, demonstrating uptake of unencapsulated ^{18}F-SKI249380 and micelle or liposome-formulated ^{18}F-SKI249380 in tumor-bearing brains (arrows) as against non–tumor-bearing (control) brain (arrowhead). **(B)** Graphical summary of tumor uptake values (%ID/g) for treatment and control groups. **(C)** Representative sagittal microPET brain images from control and tumor-bearing (arrows) animals iv injected with ^{18}F-SKI249380, before and after blocking with pharmacologic doses of dasatinib. Corresponding 1-hr time-activity curves are shown. Reprinted with the permission of the Neoplasia, Benezra et al., 2012.

Micelles are self-assembled colloidal nanoparticles with a hydrophobic core and hydrophilic shell [35]. They can passively accumulate in the areas with leaky vasculature such as tumors, inflammation, and infarction. Recently, polymer micelles are gaining an increasing attention for PET imaging due to their high stability and good biocompatibility. A special group of polymeric micelles can be synthesized by the conjugation of water-soluble copolymers with lipids (such as polyethylene glycol-phosphatidyl ethanolamine, PEG-PE). For example, Xiao et al. reported a multifunctional micelle made up with a hyperbranched amphiphilic block copolymer [36]. The unimolecular micelles were conjugated with cRGD peptide (for integrin $\alpha_v\beta_3$ target), NOTA (a macrocyclicchelator for ^{64}Cu-labeling), and doxorubicin (DOX; for cancer therapy). *In vitro* study showed a much higher cellular uptake of cRGD-conjugated micelles in U87MG human glioblastoma cells due to integrin $\alpha_v\beta_3$-mediated endocytosis than non-targeted micelles, thereby leading to a significantly higher cytotoxicity. *In vivo* PET imaging demonstrated a higher tumor accumulation of ^{64}Cu-micelle-DOX-cRGD than non-targeted control (^{64}Cu-micelle-DOX). Injection with a blocking dose of cRGD peptide along with ^{64}Cu-micelle-DOX-cRGD significantly reduced tumor uptake, indicating integrin $\alpha_v\beta_3$-specific binding of ^{64}Cu-micelle-DOX-cRGD.

Dendrimers

Dendrimers are a novel class of artificial macromolecules with a well-defined topological structure [37]. Dendrimers are usually constructed by three major components from the interior to the surface: a central core with two or more reactive groups; repeated units covalently attached to the central core and organized in a series of radially homocentric layers as called "generations"; peripheral functional groups on the surface which predominantly determine the physicochemical properties of a dendrimer. Based on the molecular "hooks" attached to the surface, dendrimers can be actively targeted to cancer cells, tumor tissues, and abnormal vessels. Additionally the nanosized dendrimers can passively accumulate in tumor tissues via the EPR effect [38]. Dendrimers can be constructed in various sizes, molecular weights, and chemical compositions. Due to the high loading capacity and the flexibility of controlling the polymer structure, dendrimers are favorable scaffolds or vehicles for the construction of imaging probes [39-45]. However, few studies about positron emitting radionuclides labeled dendrimers have been reported to date [46,47]. Recently, the Shi group has reported gadolium-loaded dendrimer-entrapped GNPs (Gd-Au DENPs) for dual mode computed tomography (CT)/magnetic resonance (MR) imaging applications. They successfully modified amine-terminated generation five poly(amidoamine) dendrimers(G5.NH_2) with gadolinium (Gd) chelator and polyethylene glycol (PEG) monomethyl ether. The multifunctional Gd-Au DENPs were formed by sequential chelation of Gd(III) and acetylation of the remaining dendrimer terminal amine groups [48]. Because the DOTA chelatorin the dendrimers can be readily labeled by positron emitting nuclides, such as ^{64}Cu, the newly developed dendrimers could afford a potential platform for PET application.

Radiolabeled nanoparticles for tumor imaging

Cancer imaging is one of major applications of radiolabeled nanoparticles in medical research. As described in the above sections, various radiolabled nanoparticles have been extensively studied for tumor imaging. Rather than focusing on the various types of nanoparticles, this section concentrates on the utilization of radiolabeled nanoparticles for imaging specific tumor biology, such as tumor angiogenesis.

In general, there are two major strategies for accumulating radiolabeled NPs in the tumor tissue. The first one is known as "passive targeting" (or spontaneous accumulation) based on the EPR effect. The second approach is called as "active targeting", meaning that NPs could target specific cancer cells or tissues by attaching with target-specific molecules. Over the past decade, numerous PET probes have been extensively explored for targeting specific biological processes in cancer biology [6]. For example, angiogenesis is a major biological process in tumor growth and metastatic spread. The characterization of angiogenesis is the formation of new capillaries by cellular outgrowth from existing microvessels [49]. Integrin $\alpha_v\beta_3$, upregulated at the sites of angiogenesis, has been proven to be a vital biomarker for cancer imaging. Linear as well as cyclic RGD peptides have been identified as integrin$\alpha_v\beta_3$-specifice ligands with high binding affinity and selectivity. Liu's group labeled RGD peptide-conjugated SWNTs with ^{64}Cu via a DOTA chelator [50]. *In vivo* PET imaging of U87MG tumor xenografts showed the specific binding of ^{64}Cu-DOTA-PEG-RGD-SWNTs to integrin $\alpha_v\beta_3$ overexpressed U87MG tumors.

Platelet-derived growth factor receptor (PDGFR) and nonreceptor membrane-associated tyrosine kinases [i.e., Src family kinases (SFKs)] have been identified as attractive candidates for targeted tumor imaging and therapeutic intervention. It is known that Dasatinib is a new generation of ATP-competitive inhibitor for PDGFR and SFKs. Benezra and co-workers reported a novel fluorinated dasatinib derivative (F-SKI249380) conjugated with nanocarriers for microPET imaging in a platelet-derived growth factor B (PDGFB)–driven genetically engineered mouse model (GEMM) [51]. PDGFR receptor status and tumor-specific targeting were non-invasively evaluated using ^{18}F-SKI249380, and ^{18}F-SKI249380–containing micellar and liposomal nanoformulations. As shown in Figure 3, the tumor uptake of ^{18}F-SKI249380–containing micelle formulations was significantly higher than that of ^{18}F-SKI249380.

The development of radio labeled NPs for dual-modality or multimodality tumor imaging, such as PET/fluorescence, PET/MRI, PET/MRI/optical imaging has gained increasing interest in recent years. Each imaging modality has its own advantages and limitations [7]. For instance, radionuclide-based imaging techniques, such as PET, are highly sensitive and quantitative but they have relatively poor spatial resolution; MRI provides high spatial resolution images with exquisite soft tissue contrast yet it suffers from low sensitivity; optical imaging can sensitively and sequentially interrogate cellular and molecular functions in living subjects, however, the energies in the visible to near-infrared region of the spectrum are limited to penetrate the depth of mammalian tissues. Therefore, combinations of imaging techniques, as so-called "multimodality imaging", are being designed to take advantage the strengths of modalities while minimizing its limitations, which as a result may simultaneously provide comprehensive biological information. In one study, integrin $\alpha_v\beta_3$ targeted IO NPs were developed for dual PET and MR tumor imaging [52]. RGD peptides were conjugated on the surface of IO NPs

where the DOTA chelators were incorporated for ^{64}Cu labeling. PET/MR imaging was carried out by using ^{64}Cu-DOTA-IO-c(RGDyK) NPs to monitor integrin $\alpha_v\beta_3$ expression levels in U87MG tumor bearing mice. Tumor uptakes of ^{64}Cu-DOTA-IO-c(RGDyK) NPs at 1 h, 4 h, and 21 h pi were much higher than those of ^{64}Cu-DOTA-IO NPs without the conjugation of RGD peptide. Pre-injection of a RGD peptide – [c(RGDyK)] significantly reduced the radioactivity uptake in tumors, suggesting the targeting specificity of ^{64}Cu-DOTA-IO-c(RGDyK) NPs. The T2-weighted MRI also showed integrin specific delivery of DOTA-IO-c(RGDyK) NPs, which was consistent with PET data. In another example, Cai et al. developed a quantum dot (QD)-based probe for dual-function near infrared fluorescence (NIRF) and PET imaging [53]. The QDs with an amine surface were modified with RGD peptides for integrin $\alpha_v\beta_3$ targeting, and DOTA chelator for ^{64}Cu labeling. In cell-based binding assay, the DOTA–RGD–QDs exhibited $\alpha_v\beta_3$ integrin specific binding in U87MG human glioblastoma cells. For *in vivo* study, the U87MG tumor uptake of ^{64}Cu-labeled DOTA–RGD–QDs was significantly higher than that of ^{64}Cu-labeled DOTA–QD. Excellent linear correlation was obtained between the results measured by PET imaging and those measured by NIRF imaging as shown in Figure 4. Histological examination further confirmed that the majority of DOTA–RGD–QDs target the tumor vasculature through an RGD–$\alpha_v\beta_3$ integrin interaction.

In a recent study, Xie and colleagues applied triple functional iron oxide nanoparticles for *in vivo* PET/NIRF/MRI study [54]. Human serum albumin (HSA)-coated iron oxide nanoparticles (HSA-IONPs) were dually labeled with ^{64}Cu-DOTA and Cy5.5, and tested

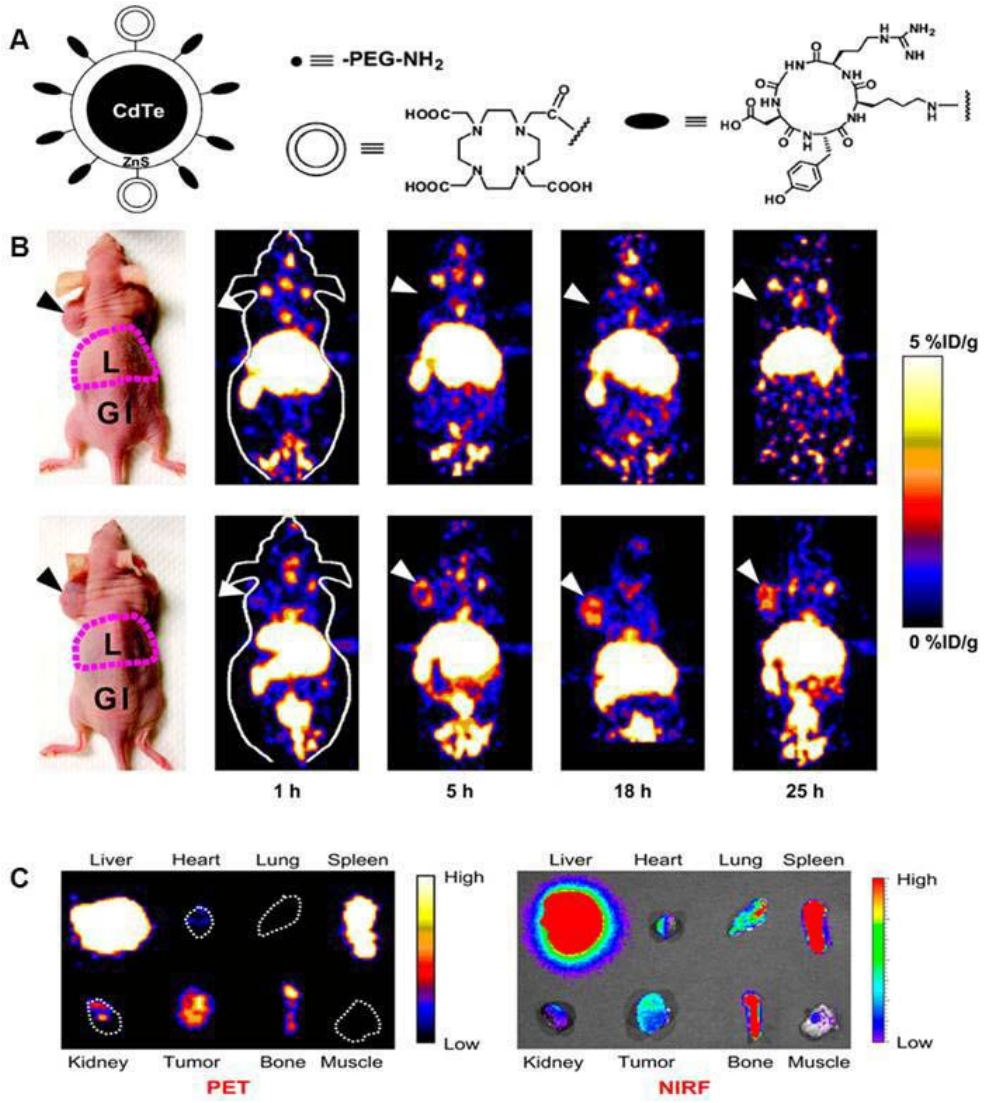

Figure 4: (A) Schematic illustration of dual-function PET/NIRF probe DOTA-QD-RGD. PEG = polyethylene glycol. **(B)** Whole-body coronal PET images of mice at 1, 5, 18, and 25 h after injection of 7-14 MBq of ^{64}Cu-labeled DOTA-QD or DOTA-QD-RGD. Arrowheads indicate tumors. Images shown are for slices that were 1 mm thick. GI = gastrointestinal tract; L = liver. **(C) Left**: PET image of harvested tissues at 5 h after injection of ^{64}Cu-labeled DOTA-QD-RGD. **Right:** NIRF image of harvested tissues at 5 h after injection of ^{64}Cu-labeled DOTA-QD or DOTA-QD-RGD. Reprinted with the permission of the Journal of Nuclear Medicine, Cai et al., 2007.

in a subcutaneous U87MG xenograft mouse model. PET/NIRF/MR tri-modality imaging, *ex vivo* study, and histological examinations demonstrated that the constructed nanosystem was suitable for dual encapsulation of IONPs and drug molecules. The HSA-IONPs labeled with ^{64}Cu and Cy5.5 manifested a prolonged circulation half-life and massive accumulation in lesions (Figure 5). With a high spatial resolution, MRI offers a better description of the particle distribution pattern than either PET or NIRF. In another hand, PET provides a better signal-to-noise ratio while NIRF can be visualized both *in vivo* by an IVIS system and *ex vivo* by fluorescence microscopy, playing a unique role of bridging the *in vivo* and histological observations. By combining the information gathered from all the aspects, it is clear that the HSA-IONPs have not only a high retention rate, but also a good extravasation rate and a low macrophage uptake rate at the tumor area.

Radiolabeled nanoparticles for cardiovascular imaging

Cardiovascular diseases include, but are not limited to, arteriosclerosis (general hardening of arteries); atherosclerosis (plaque-associated arterial hardening); thrombotic blockage stenosis and ischemia in coronary, carotid, renal and other peripheral arteries; aneurysms; venous blood clots and varicose veins; dysregulation of hemostasis (e.g., platelets and von Wille brand factor) [55]. Among these diseases, atherosclerosis is one of the most prevalent vascular disease models in which nanomedicine approaches have been studied.

Atherosclerosis, a chronic inflammatory disease of the arterial wall, is the major cause of morbidity and mortality from cardiovascular

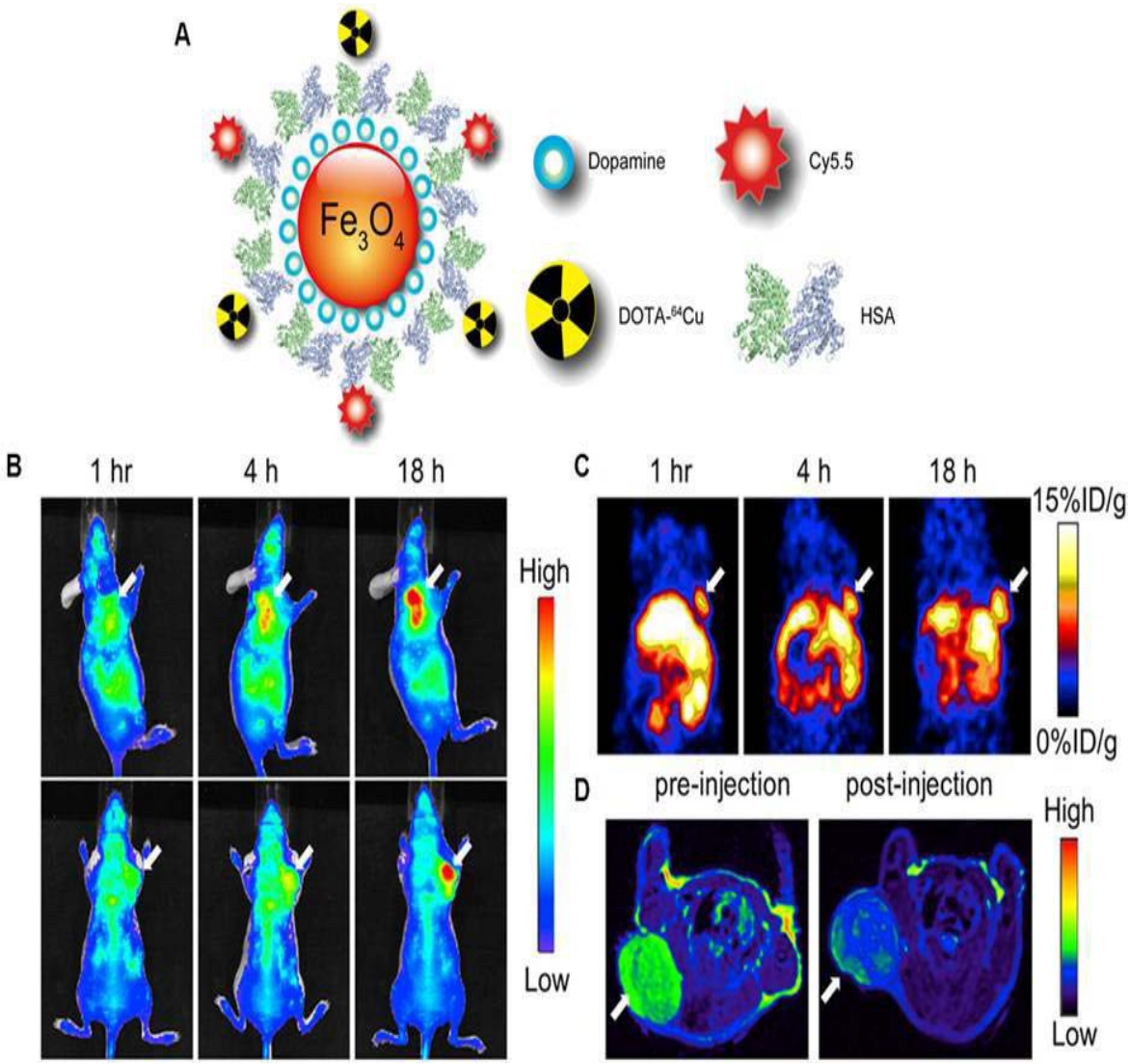

Figure 5: (A) Schematic illustration of the multi-functional HSA-IONPs. **(B)** Representative in vivo NIRF images of mouse injected with HSA-IONPs. Images were acquired 1 h, 4 h and 18 h post injection. **(C)** In vivo PET imaging results of mouse injected with HSA-IONPs. Images were acquired at 1 h, 4 h, and 18 h post injection. **(D)** MRI images acquired before the injection and at 18 h post injection. Reprinted with the permission of the Biomaterials, Xie et al., 2010.

disease. Macrophages play a central role in the atherogenic process as modulators of lipid metabolism and immune responses [56,57]. Macrophages can enter initial atherosclerotic lesions, ingest modified lipoprotein particles, and convert to foam cells at the early stage of atheroma. The accumulation of foam cells results in the formation of fatty streaks and the deposition of fibrous tissues, indicating the progression of atheroma into an intermediate stage [58]. Nahrendorf et al. developed a dextranated 20-nm nanoparticle labeled with ^{64}Cu to yield a PET, MR, and optically detectable imaging agent [59]. The radioactivity peak from PET at 24 hr after iv injection into mice deficient in apolipoprotein E with experimental atherosclerosis mapped to areas of high plaque load identified by CT, such as the aortic root and arch, and correlated with MR and optical imaging. The uptake of ^{64}Cu-labeled NPs was further confirmed by the *ex vivo* fluorescence reflectance imaging and autoradiography conducted on excised aortas.

Angiogenesis, new blood vessel formation, is a characteristic event in ischemic lesions. The overexpression of integrin $\alpha_v\beta_3$ on endothelial cells has been proven in the ischemic tissue. Almutairiet al. reported the efficacy of biodegradable dendritic structures whose surface was modified with a cyclic arginine-glycine-aspartic acid (cyclic RGD) peptide and encapsulating radioactive Bromine (^{76}Br) for PET imaging of hindlimb ischemia in a mouse model [47]. Eight tyrosine residues near the center of the macromolecular structure were functionalized for labeling with ^{76}Br. The hetero bifunctional polyethylene oxide (PEO) chains provided extended blood circulation, and cyclic RGD motifs installed at the terminal ends of the PEO chains enhanced the direct binding to $\alpha_v\beta_3$ integrin receptors. The targeted nanoprobes (IC_{50} = 0.18 nM) exhibited a 50-fold enhancement binding affinity to integrin $\alpha_v\beta_3$ over the monovalent RGD peptide alone (IC_{50} = 10.40 nM). The cell-based assay using integrin $\alpha_v\beta_3$-positive cells showed a 6-fold increase in $\alpha_v\beta_3$ receptor–mediated endocytosis for the ^{125}I-labeled dendritic nanoprobes as compared to the nontargeted nanoprobe. As shown in Figure 6, *in vivo* studies of ^{76}Br-labeled dendritic nanoprobes in a murine hindlimb ischemia model revealed highly specific accumulation of the nanoprobesin integrin $\alpha_v\beta_3$ overexpressed ischemic muscles.

In another study, Ueno et al. utilized macrophages-avid

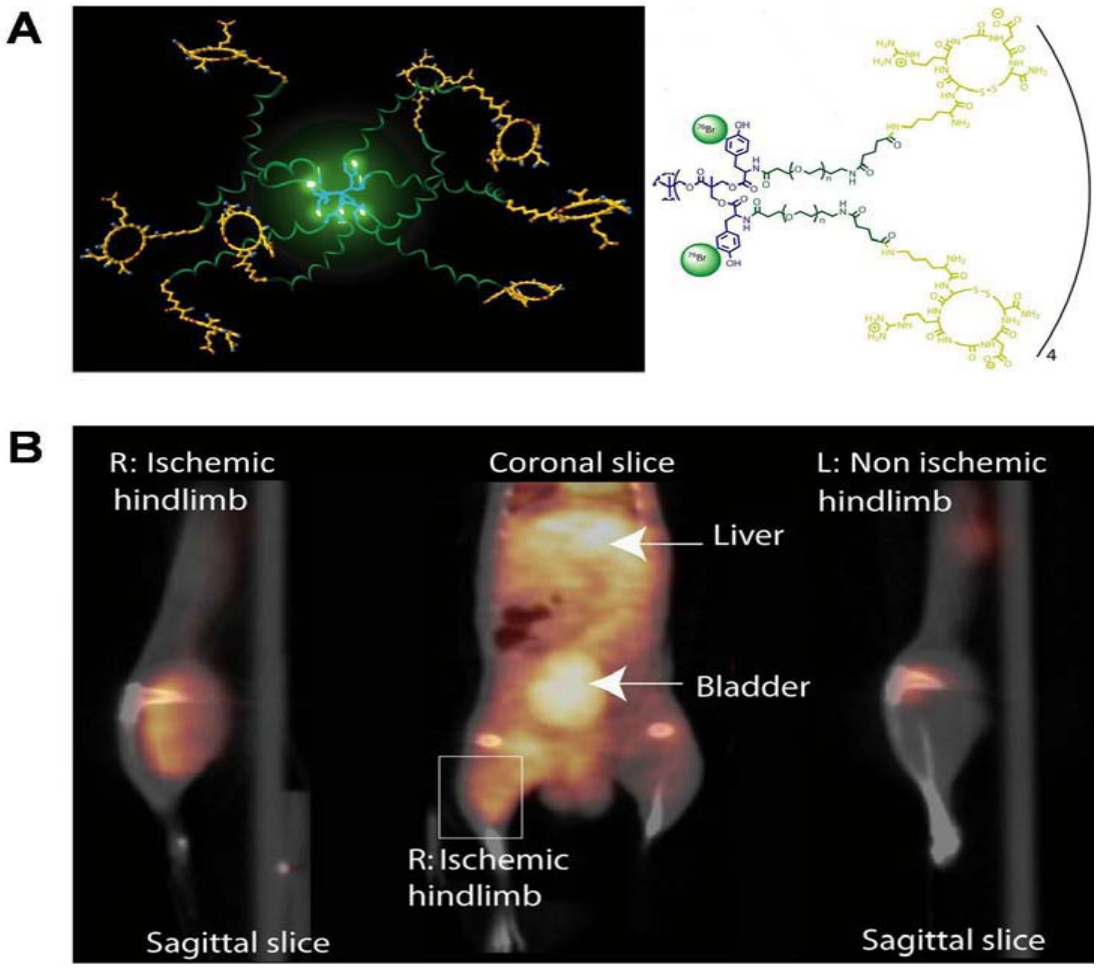

Figure 6: (A) Schematic illustration of ^{76}Br-arginine-glycine-aspartic dendritic nanoprobes for targeting integrin $\alpha_v\beta_3$. **(B)** Uptake of the ^{76}Br-labeled integrin $\alpha_v\beta_3$-targeted dendritic nanoprobes was higher in ischemic hindlimb (left side of image) than control hindlimb (right side of image).Reprinted with the permission of the Proceedings of the National Academy of Sciences of the United States of America, Almutairi et al., 2009.

nanoparticles for PET imaging to detect the rejection of heart allografts in mice [60]. The dianhydridediethylenetriaminepentaacetic acid (DTPA) conjugated cross-linked iron oxide (CLIO) NPs were coupled with Vivotag 680 and then labeled with ^{64}Cu to form the ^{64}Cu-CLIO-VT680. PET imaging was performed at 7 days after heart transplantation. C57BL/6 recipients of BALB/c allografts displayed robust PET signals. Angiotensin converting enzyme inhibitor (enalapril) significantly decreased PET signals, suggesting the probe specificity. These results demonstrated that macrophages-targeted NPs with PET imaging offered a quantitative and noninvasive method to detect both myeloid cells in allografts and their diminution after therapeutic intervention.

Conclusion and Perspectives

As a highly sensitive imaging tool, PET can assist in the translational application of nanomaterials for early stage disease detection, and monitoring of disease progression, regression, and recurrence. The good examples presented in this review demonstrated that the nanoplatforms with PET imaging could be very useful for diagnosis and treatment in cancer and cardiovascular diseases. Despite the fact that PET is highly sensitive and quantitative, it has relatively poor spatial resolution, which can be compensated by other imaging modalities, such as MRI. The beauty of nanoparticles over other materials is that they can be readily functionalized. The design of multifunctional nanoparticles could significantly improve already existing nanoparticle characteristics. Whereas monofunctional nanoparticles provide a single function, multifunctional nanoparticles can combine different functionalities in a single stable construct, which is well suitable for multimodality imaging.

Although radiolabeled NPs have shown great promise in PET imaging of diseases, several challenges need to be addressed to translate the radiolabeled NPs to clinical applications. One of the major challenges is to develop truly tissue-selective targeting NPs without the significant uptake in the mononuclear phagocytic system (MPS). To resolve this issue, the NPs can be designed with optimal surface modifications. In general, NPs coated with a hydrophilic polymer, such as PEG unit, can reduce the nanoparticle uptake in the MPS and increase circulation time as compared to the uncoated counterparts. In addition, the targeted nanocarriers functionalized with antibodies, peptides or other targeting ligands that recognize specific receptors or antigens have the potential to increase the target-to-background ratio. Considering the toxicity and immunogenicity, the biodegradable nanomaterials would be a better choice. In this regard, the organic nanomaterials are usually better than the inorganic nanoparticles. Furthermore, *in vivo* biodistribution of nanopariticles is largely dependent on the characteristics of nanoparticles, such as shape, charge, size, surface coating, and dosing [61]. Based on these factors, design considerations can be manipulated to prolong blood circulation, reduce the nonspecific distribution, and enhance imaging contrast. Moreover, in order to achieve optimal target-to-background contrast in PET, good *in vivo* stability of radiolabeled NPs is also required [8].

In conclusion, radiolabeled NPs have shown great promise in PET imaging. With the development of hybrid imaging technology, we expect that novel radiolabeled NPs with PET along with other imaging modalities will afford accurate and precise assessment of biological signatures in a real-time manner and thus improve disease management.

Acknowledgments

This work was supported by the research fund (#IRG-58-007-51) from the American Cancer Society, the Donald E. and Delia B. Baxter Foundation, USC Department of Radiology, and the Natural Science Foundation of China (Grant No. 81171368).

References

1. Kim BY, Rutka JT, Chan WC . Nanomedicine. N Engl J Med. 2010; 363: 2434-2443.
2. Weissleder R, Mahmood U . Molecular imaging. Radiology. 2001; 219: 316-333.
3. Chen K, Chen X . Design and development of molecular imaging probes. Curr Top Med Chem. 2010; 10: 1227-1236.
4. Cai W, Chen X . Multimodality molecular imaging of tumor angiogenesis. J Nucl Med. 2008; 49 Suppl 2: 113S-28S.
5. Chen K, Conti PS . Target-specific delivery of peptide-based probes for PET imaging. Adv Drug Deliv Rev. 2010; 62: 1005-1022.
6. Chen K, Chen X . Positron emission tomography imaging of cancer biology: current status and future prospects. Semin Oncol. 2011; 38: 70-86.
7. Xing Y1, Zhao J2, Conti PS3, Chen K3 . Radiolabeled Nanoparticles for Multimodality Tumor Imaging. Theranostics. 2014; 4: 290-306.
8. de Barros AB, Tsourkas A, Saboury B, Cardoso VN, Alavi A . Emerging role of radiolabeled nanoparticles as an effective diagnostic technique. EJNMMI Res. 2012; 2: 39.
9. Welch MJ, Hawker CJ, Wooley KL . The advantages of nanoparticles for PET. J Nucl Med. 2009; 50: 1743-1746.
10. Loudos G, Kagadis GC, Psimadas D . Current status and future perspectives of in vivo small animal imaging using radiolabeled nanoparticles. Eur J Radiol. 2011; 78: 287-295.
11. Kelkar SS, Reineke TM. Theranostics: combining imaging and therapy. Bioconjug Chem. 2011; 22: 1879-1903.
12. Reddy S, Robinson MK . Immuno-positron emission tomography in cancer models. Semin Nucl Med. 2010; 40: 182-189.
13. Blower PJ, Lewis JS, Zweit J . Copper radionuclides and radiopharmaceuticals in nuclear medicine. Nucl Med Biol. 1996; 23: 957-980.
14. Chen K, Wang X, Lin W, Shen K-F, Yap LP, Hughes LD et al. Strain-promoted catalyst-free click chemistry for rapid construction of 64Cu-labeled PET imaging probes. ACS Med Chem Lett. 2012; 3:1019-1023.
15. Liu Y, Welch MJ . Nanoparticles labeled with positron emitting nuclides: advantages, methods, and applications. Bioconjug Chem. 2012; 23: 671-682.
16. Ding H, Wu F . Image guided biodistribution and pharmacokinetic studies of theranostics. Theranostics. 2012; 2: 1040-1053.
17. Miller PW, Long NJ, Vilar R, Gee AD . Synthesis of ^{11}C, ^{18}F, ^{15}O, and ^{13}N radiolabels for positron emission tomography. Angew Chem Int Ed Engl. 2008; 47: 8998-9033.
18. Shokeen M, Anderson CJ . Molecular imaging of cancer with copper-64 radiopharmaceuticals and positron emission tomography (PET). Acc Chem Res. 2009; 42: 832-841.
19. Wadas TJ, Wong EH, Weisman GR, Anderson CJ . Coordinating radiometals of copper, gallium, indium, yttrium, and zirconium for PET and SPECT imaging of disease. Chem Rev. 2010; 110: 2858-2902.
20. Holland JP, Williamson MJ, Lewis JS . Unconventional nuclides for radiopharmaceuticals. Mol Imaging. 2010; 9: 1-20.

21. McDevitt MR, Chattopadhyay D, Jaggi JS, Finn RD, Zanzonico PB, Villa C, et al. PET imaging of soluble yttrium-86-labeled carbon nanotubes in mice. PLoS One. 2007; 2: e907.

22. Gong H, Peng R, Liu Z . Carbon nanotubes for biomedical imaging: the recent advances. Adv Drug Deliv Rev. 2013; 65: 1951-1963.

23. Yang K, Wan J, Zhang S, Zhang Y, Lee ST . In vivo pharmacokinetics, long-term biodistribution, and toxicology of PEGylated graphene in mice. ACS Nano. 2011; 5: 516-522.

24. Hong H, Zhang Y, Engle JW, Nayak TR, Theuer CP, Nickles RJ, et al. In vivo targeting and positron emission tomography imaging of tumor vasculature with ^{66}Ga-labeled nano-graphene. Biomaterials. 2012; 33: 4147-4156.

25. Li S, Goins B, Zhang L, Bao A. Novel Multifunctional Theranostic Liposome Drug Delivery System: Construction, Characterization, and Multimodality MR, Near-Infrared Fluorescent, and Nuclear Imaging. Bioconjug Chem. 2012; 23: 1322-1332.

26. Petersen AL, Binderup T, Rasmussen P, Henriksen JR, Elema DR, Kjaer A, et al. ^{64}Cu loaded liposomes as positron emission tomography imaging agents. Biomaterials. 2011; 32: 2334-2341.

27. Emmetiere F, Irwin C, Viola-Villegas NT, Longo V, Cheal SM, Zanzonico P, et al. ^{18}F-labeled-bioorthogonal liposomes for in vivo targeting. Bioconjug Chem. 2013; 24: 1784-1789.

28. Xie H, Wang ZJ, Bao A, Goins B, Phillips WT . In vivo PET imaging and biodistribution of radiolabeled gold nanoshells in rats with tumor xenografts. Int J Pharm. 2010; 395: 324-330.

29. Karmani L, Labar D, Valembois V, Bouchat V, Nagaswaran PG, Bol A et al. Antibody-functionalized nanoparticles for imaging cancer: influence of conjugation to gold nanoparticles on the biodistribution of ^{89}Zr-labeled cetuximab in mice. Contrast Media Mol Imaging. 2013; 8: 402-408.

30. Pérez-Campaña C, Gómez-Vallejo V, Martin A, San Sebastián E, Moya SE, Reese T et al. Tracing nanoparticles in vivo: a new general synthesis of positron emitting metal oxide nanoparticles by proton beam activation. Analyst. 2012; 137: 4902-4906.

31. Perez-Campana C, Gomez-Vallejo V, Puigivila M, Martin A, Calvo-Fernandez T, Moya SE et al. Biodistribution of different sized nanoparticles assessed by positron emission tomography: a general strategy for direct activation of metal oxide particles. ACS Nano. 2013; 7: 3498-3505.

32. ThorekDLJ, Czupryna J, Chen KA, Tsourkas A. Molecular imaging of cancer with superparamagnetic iron-oxide nanoparticles. In: Cancer Imaging: Intrumentation and Applications. Volume 2 (Hayat MA, ed), pp85-96.

33. Bouziotis P, Psimadas D, Tsotakos T, Stamopoulos D, Tsoukalas C . Radiolabeled iron oxide nanoparticles as dual-modality SPECT/MRI and PET/MRI agents. Curr Top Med Chem. 2012; 12: 2694-2702.

34. Thomas R, Park IK, Jeong YY . Magnetic iron oxide nanoparticles for multimodal imaging and therapy of cancer. Int J Mol Sci. 2013; 14: 15910-15930.

35. Torchilin VP . Micellar nanocarriers: pharmaceutical perspectives. Pharm Res. 2007; 24: 1-16.

36. Xiao Y, Hong H, Javadi A, Engle JW, Xu W, Yang Y et al. Multifunctional unimolecular micelles for cancer-targeted drug delivery and positron emission tomography imaging. Biomaterials. 2012; 33: 3071-3082.

37. Satija J, Gupta U, Jain NK . Pharmaceutical and biomedical potential of surface engineered dendrimers. Crit Rev Ther Drug Carrier Syst. 2007; 24: 257-306.

38. Cheng Y, Zhao L, Li Y, Xu T . Design of biocompatible dendrimers for cancer diagnosis and therapy: current status and future perspectives. Chem Soc Rev. 2011; 40: 2673-2703.

39. Parrott MC, Benhabbour SR, Saab C, Lemon JA, Parker S, Valliant JF et. al. Synthesis, radiolabeling, and bio-imaging of high-generation polyester dendrimers. J Am Chem Soc. 2009; 131: 2906-2916.

40. Criscione JM, Dobrucki LW, Zhuang ZW, Papademetris X, Simons M, Sinusas AJ et. al. Development and application of a multimodal contrast agent for SPECT/CT hybrid imaging. Bioconjug Chem. 2011; 22: 1784-1792.

41. Khosroshahi AG, Amanlou M, Sabzevari O, Daha FJ, Aghasadeghi MR, Ghorbani M et al. A comparative study of two novel nanosized radiolabeled analogues of methionine for SPECT tumor imaging. Curr Med Chem. 2013; 20: 123-133.

42. Xu X, Zhang Y, Wang X, Guo X, Zhang X, Qi Y et. al. Radiosynthesis, biodistribution and micro-SPECT imaging study of dendrimer-avidin conjugate. Bioorg Med Chem. 2011; 19: 1643-1648.

43. Zhang Y, Sun Y, Xu X, Zhang X, Zhu H, Huang L et. al. Synthesis, biodistribution, and microsingle photon emission computed tomography (SPECT) imaging study of technetium-99m labeled PEGylated dendrimer poly(amidoamine) (PAMAM)-folic acid conjugates. J Med Chem. 2010; 53: 3262-3272.

44. Zhang Y, Sun Y, Xu X, Zhu H, Huang L, Zhang X et. al. Radiosynthesis and micro-SPECT imaging of ^{99m}Tc-dendrimer poly(amido)-amine folic acid conjugate. Bioorg Med Chem Lett. 2010; 20: 927-931.

45. Longmire M, Choyke PL, Kobayashi H . Dendrimer-based contrast agents for molecular imaging. Curr Top Med Chem. 2008; 8: 1180-1186.

46. Kobayashi H, Wu C, Kim MK, Paik CH, Carrasquillo JA, Brechbiel MW et. al. Evaluation of the in vivo biodistribution of indium-111 and yttrium-88 labeled dendrimer-1B4M-DTPA and its conjugation with anti-Tac monoclonal antibody. Bioconjug Chem. 1999; 10: 103-111.

47. Almutairi A, Rossin R, Shokeen M, Hagooly A, Ananth A, Capoccia B et. al. Biodegradable dendritic positron-emitting nanoprobes for the noninvasive imaging of angiogenesis. Proc Natl Acad Sci U S A. 2009; 106: 685-690.

48. Wen S, Li K, Cai H, Chen Q, Shen M, Huang Y et. al. Multifunctional dendrimer-entrapped gold nanoparticles for dual mode CT/MR imaging applications. Biomaterials. 2013; 34: 1570-1580.

49. Dobrucki LW, Sinusas AJ . Imaging angiogenesis. Curr Opin Biotechnol. 2007; 18: 90-96.

50. Liu Z, Cai W, He L, Nakayama N, Chen K, Sun X et.al. In vivo biodistribution and highly efficient tumour targeting of carbon nanotubes in mice. Nat Nanotechnol. 2007; 2: 47-52.

51. Benezra M, Hambardzumyan D, Penate-Medina O, Veach DR, Pillarsetty N, Smith-Jones P et al. Fluorine-labeled dasatinib nanoformulations as targeted molecular imaging probes in a PDGFB-driven murine glioblastoma model. Neoplasia. 2012; 14: 1132-1143.

52. Lee HY, Li Z, Chen K, Hsu AR, Xu C, Xie J et.al. PET/MRI dual-modality tumor imaging using arginine-glycine-aspartic (RGD)-conjugated radiolabeled iron oxide nanoparticles. J Nucl Med. 2008; 49: 1371-1379.

53. Cai W, Chen K, Li ZB, Gambhir SS, Chen X . Dual-function probe for PET and near-infrared fluorescence imaging of tumor vasculature. J Nucl Med. 2007; 48: 1862-1870.

54. Xie J, Chen K, Huang J, Lee S, Wang J, Gao J et. al. PET/NIRF/MRI triple functional iron oxide nanoparticles. Biomaterials. 2010; 31: 3016-3022.

55. Gupta AS . Nanomedicine approaches in vascular disease: a review. Nanomedicine. 2011; 7: 763-779.

56. Lusis AJ . Atherosclerosis. Nature. 2000; 407: 233-241.

57. Glass CK, Witztum JL . Atherosclerosis. the road ahead. Cell. 2001; 104: 503-516.

58. Packard RR, Libby P . Inflammation in atherosclerosis: from vascular biology to biomarker discovery and risk prediction. Clin Chem. 2008; 54: 24-38.

59. Nahrendorf M, Zhang H, Hembrador S, Panizzi P, Sosnovik DE, Aikawa E et. al. Nanoparticle PET-CT imaging of macrophages in inflammatory atherosclerosis. Circulation. 2008; 117: 379-387.

60. Ueno T, Dutta P, Keliher E, Leuschner F, Majmudar M, Marinelli B et. al. Nanoparticle PET-CT detects rejection and immunomodulation in cardiac allografts. Circ Cardiovasc Imaging. 2013; 6: 568-573.

61. Almeida JP, Chen AL, Foster A, Drezek R . In vivo biodistribution of nanoparticles. Nanomedicine (Lond). 2011; 6: 815-835.